
Article:
Brown, N. D., Rhodes, E. J., Antinao, J. L. et al. (1 more author) (2015) Single-grain post-IR IRSL signals of K-feldspars from alluvial fan deposits in Baja California Sur, Mexico. Quaternary International, 362. pp. 132-138. ISSN 1040-6182

https://doi.org/10.1016/j.quaint.2014.10.024

Single-grain post-IR IRSL signals of K-feldspars from alluvial fan deposits in Baja California Sur, Mexico

N.D. Brown[a,*], E.J. Rhodes[a], J.L. Antinao[b], E.V. McDonald[b]

[a] *Department of Earth and Space Sciences, University of California, Los Angeles, 595 Charles Young Drive East, Box 951567, Los Angeles, CA 90095-1567, USA*

[b] *Division of Earth and Ecosystem Sciences, Desert Research Institute, 2215 Raggio Parkway, Reno, NV 89512, USA*

Abstract

Single grains of K-feldspar from alluvial fan units are dated using a more time-stable signal, the post-infrared infrared stimulated luminescence, or, 'post-IR IRSL' (Buylaert et al., 2009). A quick measurement protocol is discussed, 'fast post-IR IRSL,' that stimulates first with the IR diodes at the lower temperature and then measures grain-by-grain at the higher temperature. A criterion is offered for rejecting outlying grains based on hierarchical clustering. Single-grain fading rates are found to diverge from single-aliquot fading values, and the fading rates from the brightest subset of grains correspond well with an infinite age cobble and independent age control. Age comparison with a cosmogenic depth-profile age shows agreement at 1σ. The depositional chronology suggests that the climate responsible for regionally-extensive, upper-regime floods which aggraded the older units transitioned into a climate producing weaker channelized floods around the Late Pleistocene-Holocene transition.

Keywords: post-IR IRSL, K-feldspar, hierarchical clustering, single-grain IRSL

1. Introduction

The motivation of this project is to use luminescence dating to quantify the depositional chronology corresponding to a dramatic shift in depositional style observed for a set of alluvial fans near Cabo San Lucas, Mexico. This shift in flow conditions is preserved in the bedforms of these fans, which change from an aggradational sequence of supercritical units exhibiting sheetflow characteristics to an incisional sequence of more channelized units. This study attempts to establish the timing of this shift, the duration of fan deposition, and the time interval between units. By coupling sedimentological observations (Antinao and McDonald, 2013) with an absolute chronology (this paper), we hope to elucidate the nature of regional alluvial fan sedimentation, both in terms of dynamics (e.g., episodic sedimentation pulses or gradual accumulation) and potential climatic influences (the relative importance of synoptic patterns through time).

An ideal application of luminescence dating requires adequate luminescence characteristics, a stable dose-rate environment, a time-stable signal, and the isolation of those grains which have been completely reset

*Corresponding author

Email addresses: nathan.david.brown@ucla.edu (N.D. Brown), erhodes@ess.ucla.edu (E.J. Rhodes), jantinao@dri.edu (J.L. Antinao), eric.mcdonald@dri.edu (E.V. McDonald)

at burial. In tectonically-active areas such as this, quartz grains are typically dim owing to their recent detachment from bedrock (Preusser et al., 2006; Rhodes, 2011); feldspars, however, remain bright, but suffer from anomalous fading (Huntley and Lamothe, 2001). Recent studies, however, have demonstrated the increased stability of an infrared-stimulated luminescence (IRSL) signal measured at an elevated temperature following the traditional low-temperature IRSL, i.e., post-IR IRSL (Thomsen et al., 2008; Buylaert et al., 2009; Thiel et al., 2011; Buylaert et al., 2012). To discern the nature of dose dispersion among grains and avoid problems such as partial bleaching or multiple dose populations, single-grain or small-aliquot measurements are often necessary, especially in glacigenic or fluvial environments (Rhodes, 2007; Duller, 2008). This study therefore considers the application of post-IR IRSL to single grains of K-feldspar from alluvial fan terraces within a tectonically-active basin in Mexico.

2. Study site

The southern tip of the Baja California peninsula in Mexico (Fig. 1) has experienced a dynamic climate during the Late Quaternary due to the changing influences of three different climate systems: extra-tropical Pacific cyclones, tropical cyclones, and the North American Monsoon (Bacon et al., 2010; Antinao and McDonald, 2013). Previous work on the Quaternary paleoclimate of Baja California Sur has focused on pollen analysis (Lozano-Garcia et al., 2002), vegetation remains within packrat middens (Rhode, 2002) and geochemical and rock magnetic analysis of off-shore core records (Blanchet et al., 2007), yet the possibility of using stratigraphy to characterize the evolving depositional environment of Baja California Sur during the Late Pleistocene to Holocene transition remains largely unexplored. Resolving the depositional chronology for alluvial fan aggradation in southern Baja California may elucidate the relative importance of local climate drivers during the Late Pleistocene.

The La Paz and San José del Cabo extensional basins are associated with the nearby Gulf of California rift system and contain continental and marine strata ranging in age from early middle Miocene to recent (McCloy, 1984). Several workers have mapped the regional Cenozoic stratigraphy (McCloy, 1984; Smith, 1991), and have delimited the extent of Quaternary alluvium (Martinez-Gutierrez and Sethi, 1997), but detailed mapping of morphopedosedimentary units has only recently been undertaken (Antinao and McDonald, 2013).

Six terrace units have been mapped regionally (from oldest to youngest, Qt_1 - Qt_6) (Antinao et al., Unpublished results) (Fig. 1.b). The sedimentological features within these units demonstrate a distinct shift in the style and magnitude of deposition between units Qt_4 and Qt_5. A 13.5-meter-thick exposure of Qt_4 near San Lázaro within the San José del Cabo basin contains several structures diagnostic of supercritical flow (Koster, 1978): a transverse gravel bar, long-wavelength (15 m) antidunes, and transported boulders with diameters of about 30 cm. Assuming a similar channel width to today, these bedforms would correspond to a peak discharge of about 13,000 m^3/s. There are three discrete depositional packages within the section, but the lack of soil development between them suggests that the intervening time between packages was probably brief. Qt_4 and older units are also quite regionally extensive.

A total of 48 samples (lab codes of J0186 - J0205; J0399 - J0428; J0591) are reported in this study (two were lost in shipping, J0402 and J0411) from terrace units Qt_2 (older) - Qt_6 (younger), from a terrace deposited in 1976 and from three modern channels. At many sites, samples were collected in sequences of four to check for stratigraphic consistency in ages. Unit Qt_4 was sampled at a relatively high density (22 samples) to elucidate the internal depositional dynamics; there were 6 samples from Qt_2, 4 from Qt_3, 7 from Qt_5, 2 from Qt_6, 4 from an historic 1976 flood event, and one each from three modern channels.

3. Experimental details

3.1. Sample preparation and equipment

K-feldspar grains of 175-200 μm were isolated from the sedimentary samples under dim amber LED light conditions. Subsamples were wet-sieved, treated with 3% HCl, separated by density with lithium metatungstate (ρ <2.58 g/cm^3), and treated with 10% HF for 10 minutes to remove the outer layer from the grains. As sediments contained little organic material, treatment with H_2O_2 was considered unnecessary.

Luminescence measurements were carried out using a TL-DA-20 Risø automated reader equipped with a single-grain IR laser (830 nm, at 90% of 150 mW) (Bøtter-Jensen et al., 2003) and a $^{90}Sr/^{90}Y$ beta source. Measurements of scatter in D_e values for Risø calibration quartz suggest that source inhomogeneity causes 11% overdispersion. Emissions were detected through a Schott BG3-BG39 filter combination. Samples were mounted on aluminum single-grain discs with 100 holes.

A calibrated EG&G ORTEC MicroNOMAD portable NaI gamma spectrometer was used to determine the *in situ* gamma dose-rate for all samples near La Paz, and several samples near Cabo San Lucas. The U and Th concentrations were measured with inductively-coupled plasma mass spectrometry (ICP-MS), and the K concentration was measuring using inductively-coupled plasma optical emission spectrometry (ICP-OES)(Table 1). These values were used to calculate the total beta dose-rate contribution using the conversion factors of Adamiec and Aitken (1998). As both gamma spectrometer and ICP measurements were made, the degree of potential U-series disequilibrium could be examined; NaI gamma spectrometry detects nuclides in the lower-half of uranium and thorium decay chains, while ICP-MS measures parent nuclide concentration (Olley et al., 1996). For the majority of samples, the ratio of measured uranium concentrations were near one, and where the ICP estimate of U concentration was higher than the gamma spectrometer estimate, the Th ratios were equally high, suggesting that this effect may result from spatial inhomogeneity. Examination of the age estimates that show this effect in comparison to those from the same stratigraphic section suggests that either: a) the ICP results correct for spatial inhomogeneity on the decimeter scale and provide a representative beta dose-rate assesment, or b) the ICP results for these samples may suffer from the effects of severe sediment inhomogeneity on the millimeter scale, leading to a degree of beta dose-rate overestimation. A value of 12.5 $\pm$ 0.12 wt. % K content was used in calculating the internal dose rate (Huntley and Baril, 1997). Sediment samples were collected within each sample hole for water content measurement, and cosmic dose-rates were estimated following Prescott and Hutton (1994).

3.2. Measurement protocols

Two different post-IR IRSL (Buylaert et al., 2009) single-aliquot regenerative-dose (SAR) protocols (Murray and Wintle, 2000) were used to measure equivalent dose (D_e) values. The difference in protocols is the measurement of the IR_{50} signal; in the normal post-IR_{50} IR_{225} sequence, both the IR_{50} and the post-IR_{50} IR_{225} signals are measured using the single-grain IR laser for 3 s per grain, whereas in the 'fast' post-IR_{50} IR_{225} sequence the IR_{50} signal is measured per aliquot using the IR diodes for 100 s. This fast post-IR_{50} IR_{225} protocol saves time by evicting the more unstable charge (IR_{50}) once per aliquot, and measuring only the more stable signal (IR_{225}) grain-by-grain. The final 0.5 s are subtracted from the first 0.5 s of stimulation to define the signal intensity. Both protocols incorporate a preheat of 250 °C for 60 s before natural and regenerative measurements, as well as a stimulation with the IR diodes at 290 °C for 40 s at the end of each SAR cycle.

The difference in heat received between the first and last grain during the measurement of the post-IR IR signal was also considered. To understand the effect of prolonged heating on the signals, 200 grains of sample J0196 were given a dose of 50 Gy, then the single-grain IR_{50} signals were measured. Prior to measuring the post-IR IR signal, however, the discs were held at 225 °C for 0, 100 and 1000 s. The means of the sensitivity-corrected signals increased with heat duration by about 16% per decade, though the signals all remained within 1σ of each other; this effect is not yet understood. The dose-recovery tests for samples J0196 (Qt_3 near San José del Cabo) and J0400 (Qt_4 near La Paz) were also examined: no significant trend was observed when the recovered doses were plotted against the time held at 225 °C before stimulation, suggesting that any difference in heating between grains is probably insignificant.

4. Equivalent dose distributions

Accurately estimating the dose-frequency distribution of single grains is paramount when interpreting the depositional history of a sample (Galbraith, 2010). Variation in single-grain D_e values can be caused by a number of factors (Duller, 2008), including partial bleaching, bioturbation (Rink et al., 2013), dosimetric heterogeneity (Thomsen et al., 2003, 2005), instrument reproducibility (3.3%, Thomsen et al., 2005), and (in the case of feldspars) differential fading (Auclair et al., 2003) and/or internal dose-rates (Huntley and Baril, 1997).

A robust interpretation of sample history therefore requires a methodology. First, a reasonable overdispersion must be added in quadrature to the errors of all grains. Thomsen et al. (2005) suggest 10% as a reasonable approximation of instrumental and irradiation heterogeneity errors for single grains of quartz. For this study, we have applied an overdispersion of 15% to all age calculations. This term accounts for the intrinsic variability that any well-bleached sample should exhibit and precludes the possibility of giving too much weight to any one seemingly precise grain (Rhodes et al., 2010).

Second, any outliers must be rejected. Outlying grains may represent accidental inclusion during sampling or bioturbation. The finite mixture model (Galbraith and Green, 1990) may work well to discriminate between

several discrete dose populations, if the number of components are known and the populations are normally distributed; however, the problem of identifying individual grains as outliers, as an unknown number of singletons or multiple clustered grains which are far from the majority, remains poorly defined within the luminescence literature.

We propose using hierarchical clustering to quantify grain similarity and thereby to define a similarity threshold below which grains can be confidently rejected as statistical outliers (Duda, 1973). To do this, similarity must first be defined in terms of grain D_e values and errors. The Bhattacharyya distance (Bhattacharyya, 1946) compares two samples p and q with known means (μ_p and μ_q) and standard deviations (σ_p and σ_q):

$$D_B(p,q) = \frac{1}{4}\ln(\frac{1}{4}(\frac{\sigma_p^2}{\sigma_q^2} + \frac{\sigma_q^2}{\sigma_p^2} + 2)) + \frac{1}{4}(\frac{(\mu_p - \mu_q)^2}{\sigma_p^2 + \sigma_q^2}).$$

Samples are defined as similar when both the means and standard deviations are similar, i.e., 13.5±0.5 is closer to 12.5±0.5 than to 13.5±5.0. This ensures that precise potential neighbors are sooner clustered than imprecise ones, which are unlikely to become outliers. Conversely, when grains are precise and far from each other, the second term in the equation magnifies according to the difference in means squared over the sum of the variances. To evaluate the similarity of all grains, one can first define a matrix with D_B distances between every pair of grains, and then progressively combine the grains into clusters until only one cluster remains. The most dissimilar grain(s) can then be identified as the last cluster added.

Finally, the dose frequency distribution must be estimated. This can be done parametrically, assuming a specific distribution form and estimating the parameters from the data (e.g., central age model, minimum age models Galbraith et al., 1999). Alternately, for the minimum age of a single-grain sample it is possible to use overdispersion as a threshold for omitting grains before applying the central age model, the assumption being that a single, well-bleached population should not have an overdispersion larger than, for example, 15%. Determining the appropriate overdispersion is thus critical and this will depend on the depositional environment and the dose-rate heterogeneity for each sample.

An interpreted example is given for sample J0186 (Fig. 2). Notice the importance of measuring single grains: the synthetic aliquot D_e value of 136.5±14.9 Gy is more than twice that of the single-grain minimum age model D_e value of 58.6±4.2 Gy. Given the depositional environment, we interpret this as a partial bleaching effect. Additionally, notice the omitted grains, shown circled. Stratigraphically, this may represent bioturbation, considering that the remaining grains exhibit a 'leading edge' (Rodnight, 2006, cf. p. 210) and the resulting minimum age agrees closely with the adjacent luminescence samples in sequence. Only by using such a holistic approach which incorporates stratigraphic relationships, depositional dynamics, and luminescence characteristics can the complexities of single-grain dose distributions be interpreted.

Table 1: Dose-rate data and post-IR IRSL ages.

Unit	Field code	Lab code	Depth (m)	K (%)	Th (ppm)	U (ppm)	Measured γ dose-rate (Gy/ka)	Total dose-rate (Gy/ka)	D_e (Gy)	post-IR IRSL age (ka)
Qt_2	BA1219	J0417	5	1.9±0.1	2.5±0.1	0.72±0.04	0.883±0.003	3.12±0.13	163±13	52.2±4.8
Qt_2	BA1220	J0418	6	1.9±0.1	2.0±0.1	0.80±0.04	0.883±0.003	3.14±0.13	209±19	66.5±6.8
Qt_2	BA1221	J0419	5	2.0±0.1	6.7±0.3	1.26±0.06	1.283±0.003	3.70±0.13	218±8	58.8±3.2
Qt_2	BA1222	J0420	5	2.1±0.1	7.5±0.4	1.25±0.06	1.283±0.003	3.77±0.13	210±17	55.7±5.0
Qt_2	BA1223	J0421	1.8	1.9±0.1	6.2±0.3	0.96±0.05	1.174±0.004	3.59±0.13	225±25	62.7±7.4
Qt_2	BA1224	J0422	1.8	2.0±0.1	5.8±0.3	1.17±0.06	1.174±0.004	3.69±0.13	240±20	65.0±6.1
Qt_3	SL301	J0196	15	3.2±0.2	13.9±0.7	1.70±0.09	-	5.16±0.24	158±12	30.6±2.8
Qt_3	SL302	J0197	15.2	3.0±0.2	6.4±0.3	0.98±0.05	1.409±0.004	4.54±0.20	165±15	36.4±3.6
Qt_3	SL303	J0198	15.4	3.1±0.2	5.1±0.3	0.91±0.05	1.361±0.004	4.52±0.20	163±8	36.1±2.5
Qt_3	SL304	J0199	16.3	3.3±0.2	6.3±0.3	1.13±0.06	-	4.57±0.24	169±9	37.0±2.9
Qt_4	SJ101	J0186	2.2	3.4±0.2	6.6±0.3	1.01±0.05	-	4.78±0.25	58.6±4.2	12.3±1.1
Qt_4	SJ102	J0187	2.5	2.7±0.1	9.4±0.5	1.51±0.08	-	4.43±0.21	60.2±4.6	13.6±1.2
Qt_4	SJ103	J0188	2.82	2.8±0.1	8.7±0.4	1.21±0.06	-	4.39±0.21	63.9±4.6	14.6±1.3
Qt_4	SJ104	J0189	3.05	3.2±0.2	5.5±0.3	0.87±0.04	-	4.47±0.24	60.9±4.3	13.6±1.2
Qt_4	SJ201	J0190	0.9	3.8±0.2	6.6±0.3	0.87±0.04	1.543±0.005	5.38±0.25	16.2±1.9	3.0±0.4
Qt_4	SJ202	J0191	1.4	3.8±0.2	5.5±0.3	0.75±0.04	-	5.05±0.28	23.3±2.0	4.6±0.5
Qt_4	SJ203	J0192	2	3.0±0.2	7.8±0.4	1.02±0.05	-	4.49±0.22	31.3±4.4	7.0±1.0
Qt_4	SJ204	J0193	2.77	3.4±0.2	6.9±0.3	1.06±0.05	-	4.81±0.25	97.9±6.2	20.4±1.7
Qt_4	ST201	J0202	0.7	2.6±0.1	5.3±0.3	0.95±0.05	-	3.93±0.20	4.0±0.5	1.0±0.1
Qt_4	ST202	J0203	1.14	2.9±0.1	5.0±0.3	0.81±0.04	-	4.16±0.21	8.5±0.8	2.0±0.2
Qt_4	ST203	J0204	1.6	3.0±0.2	4.5±0.2	0.85±0.04	-	4.23±0.22	20.4±1.8	4.8±0.5
Qt_4	ST204	J0205	2.48	2.0±0.1	7.6±0.4	1.08±0.05	-	3.51±0.16	57.8±9.5	16.4±2.8
Qt_4	BA1201	J0399	4	1.6±0.1	1.8±0.1	0.50±0.03	0.621±0.002	2.64±0.11	27.4±3.9	11.8±2.2[1]
Qt_4	BA1202	J0400	4.2	1.7±0.1	1.4±0.1	0.38±0.02	0.608±0.002	2.67±0.12	38.2±5.7	16.4±2.9[1]
Qt_4	BA1203	J0401	4.4	1.6±0.1	1.5±0.1	0.37±0.02	0.610±0.002	2.59±0.11	30.5±6.0	13.4±3.1[1]

[1]Values were corrected using g_{2700s}=1.6±0.7.

[2]Values were corrected using g_{2700s}=3.4±0.2.

(Table 1, continued.)

Unit	Field code	Lab code	Depth (m)	K (%)	Th (ppm)	U (ppm)	Measured γ dose-rate (Gy/ka)	Total dose-rate (Gy/ka)	D_e (Gy)	post-IR IRSL age (ka)
Qt_4	BA1209	J0407	1.04	2.0±0.1	6.3±0.3	3.74±0.19	1.363±0.004	4.16±0.14	17.1±2.4	5.5±0.8[2]
Qt_4	BA1210	J0408	1.2	2.1±0.1	6.2±0.3	3.62±0.18	1.424±0.004	4.25±0.14	19.4±4.1	6.1±1.3[2]
Qt_4	BA1211	J0409	1.4	2.1±0.1	6.2±0.3	3.48±0.17	1.434±0.004	4.20±0.14	27.9±3.8	8.9±1.2[2]
Qt_4	BA1212	J0410	1.6	1.8±0.1	4.9±0.2	3.00±0.15	1.208±0.004	3.74±0.12	32.1±5.3	11.6±2.1[2]
Qt_4	BA1214	J0412	2.6	1.8±0.1	5.0±0.3	3.34±0.17	1.282±0.004	3.84±0.12	57.8±9.8	20.7±3.7[2]
Qt_4	BA1215	J0413	0.4	2.1±0.1	6.4±0.3	3.25±0.16	1.412±0.003	4.23±0.15	105±13.9	34.6±4.7[2]
Qt_4	BA1216	J0414	1.08	2.1±0.1	6.3±0.3	3.84±0.19	1.345±0.003	4.13±0.14	90.4±12	30.4±4.4[2]
Qt_5	SL401	J0200	0.5	2.6±0.1	10.3±0.5	1.98±0.10	1.363±0.004	4.56±0.18	2.3±0.5	0.5±0.1
Qt_5	SL402	J0201	0.9	2.8±0.1	8.7±0.4	1.74±0.09	1.363±0.004	4.63±0.19	1.7±0.3	0.4±0.1
Qt_5	BA1217	J0415	1.17	1.0±0.1	2.2±0.1	0.97±0.05	0.608±0.003	2.33±0.08	12.3±2.6	6.0±1.3[1]
Qt_5	BA1218	J0416	1.95	0.8±0.04	3.6±0.2	0.88±0.04	0.572±0.003	2.13±0.07	18.5±5	9.9±2.7[1]
Qt_5	BA1225	J0423	0.75	2.9±0.1	3.7±0.2	0.84±0.04	1.363±0.004	4.50±0.19	2.2±0.3	0.5±0.1
Qt_5	BA1226	J0424	0.75	3.0±0.2	3.4±0.2	0.95±0.05	1.363±0.004	4.57±0.2	1.3±0.2	0.3±0.05
Qt_5	BA1227	J0425	0.47	2.4±0.1	8.5±0.4	1.09±0.05	1.421±0.004	4.30±0.16	1.6±0.3	0.4±0.1
Qt_6	SL101	J0194	0.8	2.8±0.1	3.7±0.2	0.78±0.04	1.421±0.004	4.47±0.19	1.6±0.3	0.4±0.1
Qt_6	SL102	J0195	2	3.3±0.2	4.1±0.2	0.87±0.04	1.421±0.004	4.83±0.21	2.0±0.4	0.4±0.1
1976	BA1205	J0403	0.69	1.9±0.1	1.3±0.1	0.45±0.02	0.709±0.003	3.01±0.13	0.4±0.1	0.1±0.1[1]
1976	BA1206	J0404	0.96	1.7±0.1	2.6±0.1	0.80±0.04	0.718±0.003	2.93±0.12	1.9±1.6	0.7±0.5[1]
1976	BA1207	J0405	1.63	1.8±0.1	0.9±0.05	0.43±0.02	0.666±0.003	2.86±0.12	0.9±0.4	0.3±0.1[1]
1976	BA1208	J0406	2.84	1.7±0.1	3.0±0.2	0.86±0.04	0.639±0.003	2.83±0.12	0.9±0.2	0.3±0.1[1]
Modern	BA1228	J0426	0.1	1.8±0.1	0.6±0.03	0.26±0.01	-	2.71±0.17	-0.2±0.2	-0.1±0.1
Modern	BA1229	J0427	0.1	1.9±0.1	5.1±0.3	3.35±0.17	-	3.68±0.18	2.3±0.2	0.8±0.2[2]
Modern	BA1230	J0428	0.1	2.2±0.1	18±0.9	1.51±0.08	1.543±0.005	4.55±0.18	-4.1±0.7	-0.9±0.2

[1]Values were corrected using g_{2700s}=1.6±0.7.

[2]Values were corrected using g_{2700s}=3.4±0.2.

5. Results

5.1. Dose recovery test

To test the protocol, two samples from different regions (J0196 near Cabo San Lucas and J0400 to the east of La Paz) were first bleached for 5 hours in natural sunlight, then given doses similar to the estimated burial doses (174.5 and 46.5 Gy, respectively). After receiving a dose and preheat, the samples rested for about 40 hours prior to measurement. When measured with the post-IR IR dating protocol, the doses recovered were 172.4±3.6 (overdispersion of 14%) and 47.2±1.6 Gy (overdispersion of 11%), both within 1σ of the doses administered. The measured overdispersions add confidence to our assumption that well-bleached and uniformly dosed populations should exhibit overdispersion values close to 15%.

5.2. Anomalous fading characteristics

When selecting the post-IR IRSL stimulation temperature, two issues arise: lower temperatures probe signals which are potentially less stable, and higher temperatures probe signals which are less bleachable (Thomsen et al., 2008; Buylaert et al., 2009; Li and Li, 2011; Buylaert et al., 2012). Considering the rapid, subaqueous depositional environment of this study, we have chosen a post-IR IRSL stimulation temperature of 225 °C for 3 s, which is more bleachable than the post-IR $IRSL_{290}$, though perhaps less stable.

To assess the post-IR IRSL signal stability, we measured the sensitivity-corrected luminescence intensities of single grains and single aliquots after laboratory storage (Huntley and Lamothe, 2001). For six samples (J0196, J0400, J0407-J0410), grains were allowed to sit for a range of times, between about 2700 s to about 8 days. The fading values were generally internally consistent within 1 or 2σ (Fig. 3.a). Single aliquots were allowed to sit for up to about 6 months (Fig. 3.b). Fading values for the same sample were not always consistent when calculated using these different approaches (i.e., single grains compared with single aliquots). Sample J0196, for example, showed consistency when the weighted mean fading value of all grains were considered (n=125), but when only the grains with a test dose response greater than exp(9) were considered (n=14), the apparent g_{2700s} value (the amount of sensitivity-corrected signal lost to quantum tunneling over an order-of-magnitude increase in time, i.e., 'a decade'; Aitken, 1985, Appendix F) dropped from about 1% loss per decade to slightly less than 0 (Fig. 3.c).

To resolve this discrepancy, a granodiorite cobble sample, J0591, taken from the same region as J0196, was crushed and analyzed; it is reasonable to assume that this cobble represents the provenance material for J0196, which comes from the catchment near Cabo San Lucas (Fig. 1.a). Nine small aliquots (not single-grain discs) of this "infinite age" sample were prepared: for three, no dose was added; for three, a beta dose of 213 Gy was added to the natural; and for three, a dose of 425 Gy was added to the natural. All discs were then measured with the post-IR IR protocol. The first-cycle, sensitivity-corrected intensities (natural and natural-plus-beta signals) are shown in Fig. 3.d. The IR_{50} signal grows significantly with dose (as saturation may not be reached by adding 425 Gy, it is impossible to say the level of saturation, but there is a 32% growth in signal between 0 and 425 Gy added). The post-IR IR_{225} signal, however, is indistinguishable from

the other dose points, suggesting that field saturation is identical to laboratory saturation, i.e., fading is negligible. Since this cobble, which should be in full field saturation, appears not to fade, we can conclude that perhaps the brightest grains are most representative of a sample's true fading characteristics (e.g., that the post-IR IR_{225} signal does not fade for these granodiorite-sourced samples).

It is interesting to note that for Fig. 3.c, the summed intensities of the brightest grains do not overwhelm the dimmer grains; those with a test dose response greater than exp(10) comprise only 9% of the total intensity for grains yielding fading results and grains giving a signal greater than exp(9) comprise 47%. Therefore, the suggestion that brighter grains are more representative of fading characteristics does not simply mean that the other grains do not contribute to the infinite age signal intensity. For this study, the brightest quartile of grains were used to estimate fading characteristics of samples. The measured g-values varied regionally, but, for the samples for which g-values were measured, were consistent within each region (the samples also showed a strong, likely related, regional clustering for U, Th, and K content, suggesting the significance of provenance on sample characteristics). For samples near Cabo San Lucas, no fading corrections were made; for samples taken from the northwest, sourced by the Tertiary sandstone in Fig. 1.a, a g_{2700s} value of 3.4±0.2 was used; for the samples sourced by the Cretaceous granite in the northeast, a g_{2700s} value of 1.6±0.7 was used (Table 1).

5.3. Comparison with independent age estimate

To test the reliability of our protocol, fan sediment samples were collected for ^{10}Be depth-profile cosmogenic nuclide dating (Antinao et al., Unpublished results). Samples were taken from Qt_2 south of La Paz. Single-grain K-feldspar post-IR IRSL ages (uncorrected for fading) from samples J0417 (finite mixture model assuming 2 components with an overdispersion of 15%) and J0418 (central age model, overdispersion calculated to be 9.2%) agree with the ^{10}Be depth-profile age for pit EAO-3 (8 samples modeled after Hidy et al. (2010)) with 1000 Monte Carlo runs) at 1σ: 52.2 ± 4.8 ka (J0417), 66.5 ± 6.8 ka (J0418), and $54.0^{+10.6}_{-7.8}$ ka (EAO-3) (Antinao et al., Unpublished results) (Fig. 4). Notice the possibility to discriminate two apparent dose populations in sample J0417, the older of which can be excluded considering the single population within the stratigraphically-lower sample J0418. Such agreement with independent age control suggests that anomalous fading does not significantly obscure accurate age recovery back to at least 60 ka.

5.4. Post-IR IRSL ages and discussion

Sample dosimetric information and ages are reported in Table 1. Depositional ages are usually presumed to be minimum ages, as modeled by minimum age models, assuming an overdispersion of 15%, and occasionally rejecting outliers using the method described above. The finite mixture model was used when discrete populations were apparent (J0417, J0421-J0422) and the central age model was used when overdispersion was low and distribution was roughly gaussian (J0412-J0414; J0418). Fading corrections have been applied as by region as described in Section 5.2, according to the most sensitive quartile of grains. Agreement with

independent age control for the oldest reported unit reinforces the assertion that the fading correction for the southern samples is unnecessary.

One noticeable feature of the stratigraphic chronology presented in Table 1 is the range of age values reported for Qt_4, from 1.0 to 34.6 ka. By considering only samples taken from depths greater than 2 meters below the surface, this range becomes 11.8 to 34.6 ka. These younger ages may reflect shallow deposits coming from smaller basins in the mountain fronts, spreading over the larger fan terraces as thin layers, though the soils seem to have been forming throughout the Holocene, which discourages this hypothesis; so, the interpretation here remains open. The older ages are within 1σ of Qt_3, suggesting perhaps a continuous transition.

The depositional chronology presented in this study suggests a dichotomy between recent (past 500 years) spatially-restricted alluvial deposits, and Late Pleistocene upper-regime aggradational events. This likely reflects the Late Pleistocene-Holocene transition from a regime dominated by tropical cyclones and El Nino-enhanced zonal winter storms into a regime more similar to modern, with more subdued ENSO strength and with weakened tropical cyclone activity (Antinao and McDonald, 2013).

6. Conclusions

The application of K-feldspar single-grain post-IR IRSL to alluvial fan units appears feasible. Distributions of D_e values seem to be reducible to depositional ages which show stratigraphic consistency. Clustering analysis using the Bhattacharyya distance may prove useful for identifying statistical outliers in dose distributions. Dose-recovery test results suggest that overdispersion values of about 15% are typical of some well-bleached populations. Agreement between post-IR IRSL and ^{10}Be depth-profile ages, saturation of provenance cobbles, and single-grain fading rates all indicate that *in situ* fading is negligible for samples collected near San José del Cabo, though samples collected farther north appear to suffer minor fading. Fading values derived from the brightest grains may be most representative of a sample's true fading characteristics.

Acknowledgements

We are grateful to the NSF for project funding. We also thank Wendy Barrera for assistance in the field. Finally, reviewers Joel Spencer and Shannon Mahan are thanked for providing insightful comments which greatly improved the clarity of this manuscript.

References

Adamiec, G., Aitken, M., 1998. Dose-rate conversion factors: update. Ancient TL 16, 37–50.

Aitken, M., 1985. Thermoluminescence Dating. Academic Press, London.

Antinao, J.L., McDonald, E., 2013. An enhanced role for the Tropical Pacific on the humid Pleistocene-Holocene transition in southwestern North America . Quaternary Science Reviews 78, 319–341.

Antinao, J.L., McDonald, E., Rhodes, E.J., Brown, N.D., Barrera, W., Gosse, J.C., Zimmermann, S., Unpublished results. Late Pleistocene-Holocene alluvial stratigraphy of southern Baja California, Mexico.

Auclair, M., Lamothe, M., Huot, S., 2003. Measurement of anomalous fading for feldspar IRSL using SAR. Radiation Measurements 37, 487–492.

Bacon, S.N., McDonald, E.V., Caldwell, T.G., Dalldorf, G.K., 2010. Timing and distribution of alluvial fan sedimentation in response to strengthening of late Holocene ENSO variability in the Sonoran Desert, southwestern Arizona, USA. Quaternary Research 73, 425–438.

Bhattacharyya, A., 1946. On a measure of divergence between two multinomial populations. Sankhy: The Indian Journal of Statistics (1933-1960) 7, 401–406.

Blanchet, C.L., Thouveny, N., Vidal, L., Leduc, G., Tachikawa, K., Bard, E., Beaufort, L., 2007. Terrigenous input response to glacial/interglacial climatic variations over southern Baja California: a rock magnetic approach. Quaternary Science Reviews 26, 3118 – 3133.

Bøtter-Jensen, L., Andersen, C., Duller, G., Murray, A., 2003. Developments in radiation, stimulation and observation facilities in luminescence measurements. Radiation Measurements 37, 535–541.

Buylaert, J., Murray, A., Thomsen, K., Jain, M., 2009. Testing the potential of an elevated temperature IRSL signal from K-feldspar. Radiation Measurements 44, 560–565.

Buylaert, J.P., Jain, M., Murray, A.S., Thomsen, K.J., Thiel, C., Sohbati, R., 2012. A robust feldspar luminescence dating method for Middle and Late Pleistocene sediments. Boreas 41, 435–451.

Duda, R.O., 1973. Pattern classification and scene analysis. Wiley & Sons, Inc.

Duller, G., 2008. Single-grain optical dating of Quaternary sediments: why aliquot size matters in luminescence dating. Boreas 37, 589–612.

Galbraith, R., 2010. On plotting OSL equivalent doses. Ancient TL 28, 1–9.

Galbraith, R., Green, P., 1990. Estimating the component ages in a finite mixture. International Journal of Radiation Applications and Instrumentation. Part D. Nuclear Tracks and Radiation Measurements 17, 197–206.

Galbraith, R.F., Roberts, R.G., Laslett, G.M., Yoshida, H., Olley, J.M., 1999. Optical dating of single and multiple grains of quartz from Jinmium rock shelter, northern Australia: Part i, experimental design and statistical models. Archaeometry 41, 339–364.

Hidy, A.J., Gosse, J.C., Pederson, J.L., Mattern, J.P., Finkel, R.C., 2010. A geologically constrained Monte Carlo approach to modeling exposure ages from profiles of cosmogenic nuclides: An example from Lees Ferry, Arizona. Geochemistry, Geophysics, Geosystems 11, Q0AA10.

Huntley, D., Baril, M., 1997. The k content of the k-feldspar being measured in optical dating or in thermoluminescence dating. Ancient TL 15, 11–13.

Huntley, D.J., Lamothe, M., 2001. Ubiquity of anomalous fading in K-feldspars and the measurement and correction for it in optical dating. Canadian Journal of Earth Sciences 38, 1093–1106.

INEGI, 1987a. Carta Geologica, La Paz, Mexico, Instituto Nacional de Estadistica, Geographica e Informatica, scale 1:250,000.

INEGI, 1987b. Carta Geologica, San Jose Del Cabo, Mexico, Instituto Nacional de Estadistica, Geocrafia, e Informatica, scale 1:250,000.

Koster, E., 1978. Transverse ribs: their characteristics, origin and paleohydraulic significance, in: Miall, A. (Ed.), Fluvial Sedimentology VI. Canadian Society of Petroleum Geologists Memoirs. volume 5, pp. 161–186.

Li, B., Li, S.H., 2011. Luminescence dating of K-feldspar from sediments: A protocol without anomalous fading correction. Quaternary Geochronology 6, 468–479.

Lozano-Garcia, M.S., Ortega-Guerrero, B., Sosa-Najera, S., 2002. Mid- to Late-Wisconsin Pollen Record of San Felipe Basin, Baja California . Quaternary Research 58, 84–92.

Martinez-Gutierrez, G., Sethi, S., 1997. Miocene-Pleistocene sediments within the San Jose del Cabo Basin, Baja California Sur, Mexico, in: Johnson, M., Ledesma-Vazquez, J. (Eds.), Pliocene Carbonates and Related Facies Flanking the Gulf of California, Baja California, Mexico, Geological Society of America.

McCloy, C., 1984. Stratigraphy and depositional history of the San Jose del Cabo trough, Baja California Sur, Mexico, in: Frizzell, Jr., V. (Ed.), Geology of the Baja California peninsula, Field Trip Guidebook, San Diego Society of Economic Paleontologists and Mineralogists, Pacific Section. pp. 237–267.

Murray, A., Wintle, A., 2000. Luminescence dating of quartz using an improved single-aliquot regenerative-dose protocol. Radiation Measurements 32, 57–73.

Olley, J.M., Murray, A., Roberts, R.G., 1996. The effects of disequilibria in the uranium and thorium decay chains on burial dose rates in fluvial sediments. Quaternary Science Reviews 15, 751–760.

Prescott, J., Hutton, J., 1994. Cosmic ray contributions to dose rates for luminescence and ESR dating: Large depths and long-term time variations. Radiation Measurements 23, 497–500.

Preusser, F., Ramseyer, K., Schluchter, C., 2006. Characterisation of low OSL intensity quartz from the New Zealand Alps . Radiation Measurements 41, 871–877.

Rhode, D., 2002. Early Holocene Juniper Woodland and Chaparral Taxa in the Central Baja California Peninsula, Mexico . Quaternary Research 57, 102–108.

Rhodes, E., 2007. Quartz single grain OSL sensitivity distributions: implications for multiple grain single aliquot dating. Geochronometria 26, 19–29.

Rhodes, E.J., 2011. Optically stimulated luminescence dating of sediments over the past 200,000 years. Annual Review of Earth and Planetary Sciences 39, 461–488.

Rhodes, E.J., Fanning, P.C., Holdaway, S.J., 2010. Developments in optically stimulated luminescence age control for geoarchaeological sediments and hearths in western new south wales, australia. Quaternary Geochronology 5, 348 – 352. 12th International Conference on Luminescence and Electron Spin Resonance Dating (LED 2008).

Rink, W.J., Dunbar, J.S., Tschinkel, W.R., Kwapich, C., Repp, A., Stanton, W., Thulman, D.K., 2013. Subterranean transport and deposition of quartz by ants in sandy sites relevant to age overestimation in optical luminescence dating. Journal of Archaeological Science 40, 2217–2226.

Rodnight, H., 2006. Developing a luminescence chronology for late Quaternary fluvial change in South Africa floodplain wetlands. Ph.D. thesis. University of Wales, Aberystwyth.

Smith, J., 1991. Cenozoic marine mollusks and paleogeography of the Gulf of California, in: Dauphin, J., Simoneit, B. (Eds.), The Gulf and Peninsular Province of the Californias, American Association of Petroleum Geologists Memoir. pp. 636–666.

Thiel, C., Buylaert, J.P., Murray, A., Terhorst, B., Hofer, I., Tsukamoto, S., Frechen, M., 2011. Luminescence dating of the stratzing loess profile (austria)–testing the potential of an elevated temperature post-IR IRSL protocol. Quaternary International 234, 23–31.

Thomsen, K., Jain, M., Bøtter-Jensen, L., Murray, A., Jungner, H., 2003. Variation with depth of dose distributions in single grains of quartz extracted from an irradiated concrete block. Radiation Measurements 37, 315–321.

Thomsen, K., Murray, A., Bøtter-Jensen, L., 2005. Sources of variability in OSL dose measurements using single grains of quartz. Radiation Measurements 39, 47–61.

Thomsen, K., Murray, A., Jain, M., Bøtter-Jensen, L., 2008. Laboratory fading rates of various luminescence signals from feldspar-rich sediment extracts. Radiation Measurements 43, 1474–1486.

List of Figures

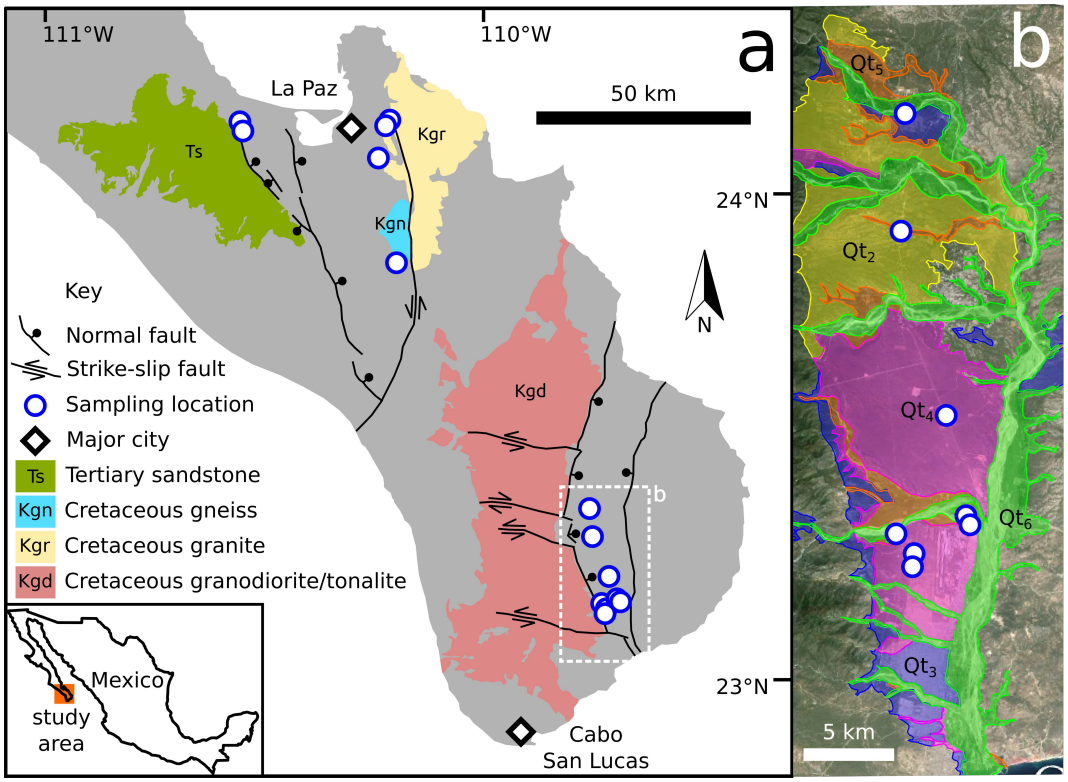

Figure 1: (a) Sampling locations shown as blue circles along with the major geologic provenances and structural features, modified from INEGI (1987a,b). Notice the three distinct groups of source regions. (b) Mapped Quaternary alluvial terraces near Cabo San Lucas along with sampling sites at each unit. Terraces mapped by Antinao et al. (Unpublished results).

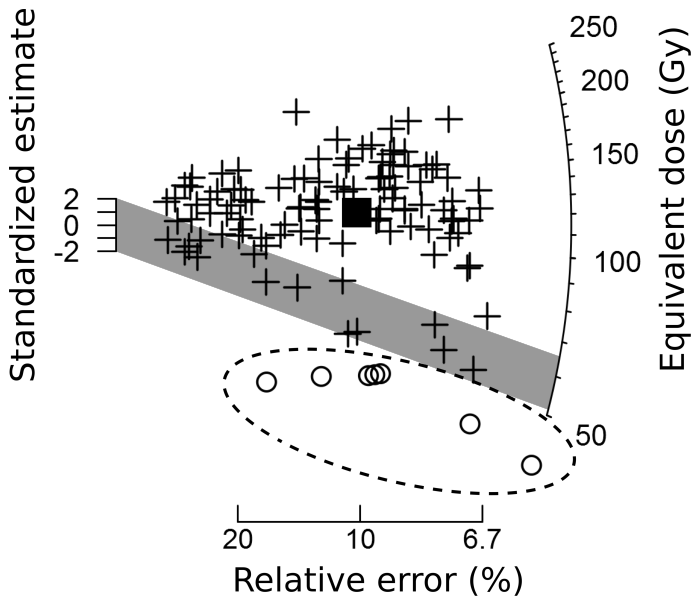

Figure 2: Sample J0186 is plotted with potentially bioturbated grains circled. The minimum age model result (calculated without the circled outliers) is displayed as a shaded region and the synthetic aliquot result is shown as the solid box.

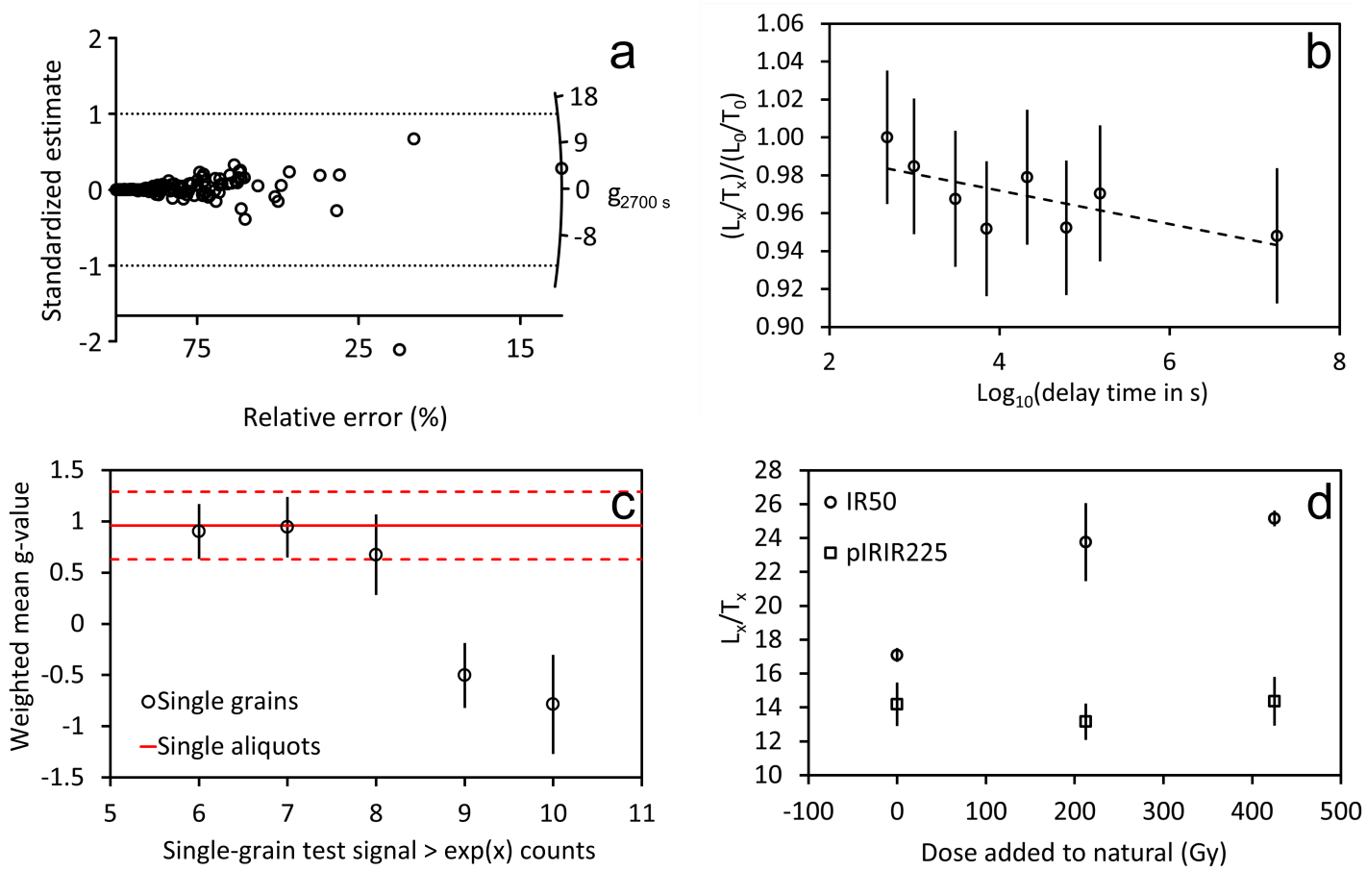

Figure 3: (a) Single-grain fading values are shown for sample J0196. Note that except for one value, all grains are consistent with no fading at 1σ, though the precision is poor. (b) For a single aliquot of the same sample (J0196), normalized fade points are shown following delays ranging from 475 s to nearly 6 months. The g_{475s} value of 0.9 ± 0.4 % loss per decade is shown as a dashed line. (c) Weighted mean of single-grain fading values with test signals greater than exp(x) are compared with the single-aliquot fading value (n=2) for J0196. The brighter grains appear not to fade, although the negative values are not fully understood. Note that the time constants are different for the two g-values: 475 s for the aliquots and about 2700 s for single grains. (d) Beta doses were added to the natural signals of aliquots of J0591, a granodiorite cobble taken near sample J0196 and assumed to be its provenance material. The points shown on (d) are the average of 3 aliquots (i.e., 9 aliquots were measured). The IR_{50} signals grow significantly with dose, while the post-IR IR_{225} natural signals are indistinguishable from the natural-plus-dose signals, suggesting that the post-IR IR_{225} signal has not faded, i.e., that the signal produced by field saturation is the same as that produced by laboratory saturation.

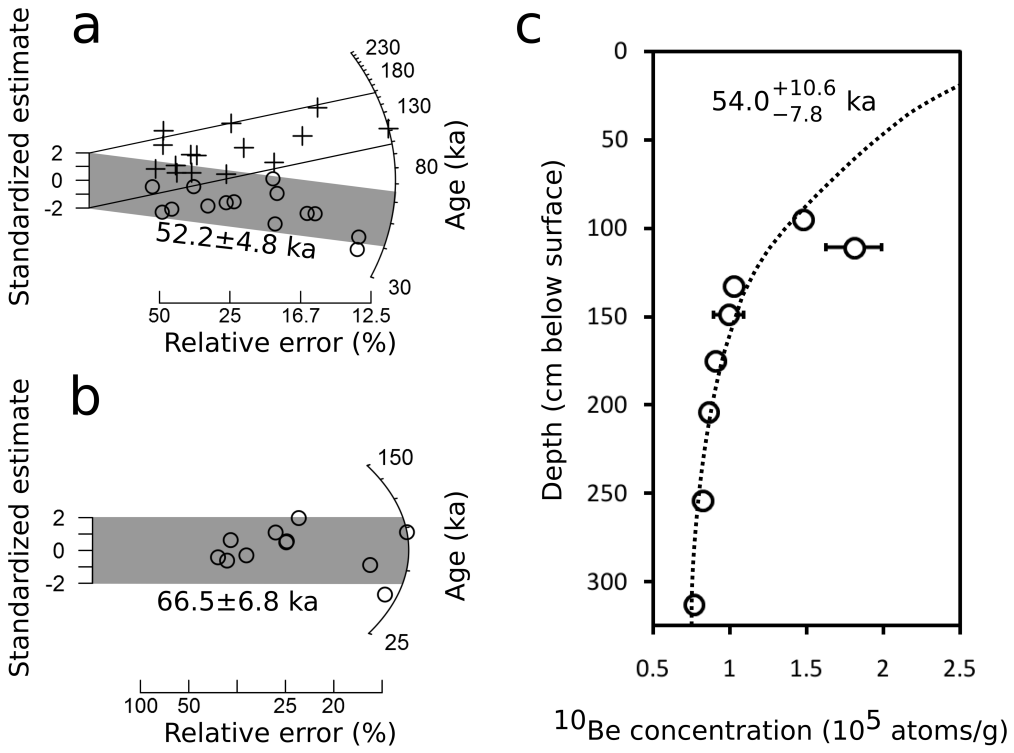

Figure 4: (a) Finite mixture model results for sample J0417, (b) central age model result for sample J0418, and (c) depth-profile age model results for the pit EAO-3 (Antinao et al., Unpublished results).